



Full length article

BELLO: A post-processing tool for the local-order analysis of disordered systems

Behnood Dianat ^{a,b}, Francesco Tavanti ^b, Andrea Padovani ^c, Luca Larcher ^c, Arrigo Calzolari ^{b,*}^a Dipartimento di Scienze e Metodi dell'Ingegneria, Università di Modena and Reggio Emilia, Via Giovanni Amendola, 2, 42122 Reggio Emilia, Italy^b CNR-NANO Istituto Nanoscienze, Centro S3, Via Campi 213A, 41125 Modena, Italy^c AMAT - Applied Materials Italia, Via Meuccio Ruini 74L, Reggio Emilia, Italy

ARTICLE INFO

Keywords:
 Python code
 Disordered systems
 Molecular dynamics
 Local-order structures
 Statistical analysis

ABSTRACT

The characterization of the atomic structure of disordered systems, such as amorphous, glasses and (bio)molecule in solution, is a fundamental step for most theoretical investigations. The properties of short- and medium-range local order structures are responsible for the electronic, optical and transport properties of these systems. Here, we present the BELLO open source code, a post-processing script-tool created for the automatic analysis and extraction of structural characteristics of disordered and amorphous systems. BELLO is agnostic to the code that generated single configurations or trajectories, it provides an intuitive access through a graphical user interface (GUI), and it requires minimal computational resources. Its capabilities include the calculation of the order parameter q , the folded structure identification, and statistical analysis tools such as atomic coordination number and pair/angle-distribution functions. The working principles of the code are described and tested on *ab initio* molecular dynamics trajectories of amorphous chalcogenides.

1. Introduction

Non-crystalline solids showed a rapidly growing interest for their photonic, nanoelectronic, and memory applications. These include, e.g., amorphous H:Si, chalcogenides, and amorphous metal-oxides for solar cells [1,2], optical amplifiers [3] thin-film transistors [4,5], optical fibers [6], sensors [7], storage DVDs [8], and memories [9,10]. The common characteristics of these materials is the disordered atomic structure, i.e. the lack of translational invariance. This usually implies peculiar properties such as homogeneity and isotropy, nanoscale structure control, large sample dimensions, more flexibility and lower density with respect to the corresponding crystalline phases. At the same time, disorder affects most of the electronic and transport properties of these materials [11]. For example, in disordered semiconductors electrons and holes close to the band edges are localized [12,13]. As a consequence, the mobility in amorphous systems becomes smaller than that in the corresponding crystal. Similar considerations holds for other physical properties, such as the localization of lattice vibrations that causes the drop of the thermal conductivity in amorphous phase.

The microscopic origin of these characteristics is intimately related to the formation of local-order structures within the sample. Indeed, even though it is impossible to envisage a unique atomic configuration for a disordered compound, amorphous and glass structures are not completely random, as that in an ideal gas. At the atomic scale,

non-crystalline solids are characterized by so-called *normal bonding* structures and defects [14]. The former describe atom connection that exists also in the corresponding crystal; the latter refer to ill-atomic coordination, such as dangling and *wrong* bonds that do not exist in the crystal [15]. The normal bonding structure can further be divided into the short (< 0.5 nm) and the medium-range (0.5–3.0 nm) structures [16]. Short range structures are mostly determined by three main parameters: the coordination number Z of atoms, the bond length r , and the bond angle θ . The coordination number is a direct consequence of the electron configuration and the chemical composition of the system that may cause the formation of both homopolar and heteropolar bonds. The bond length r increases in proportion to size of the atomic species. Bond angles keep into account the bond distortions and quantify the variance to the ideal crystal structure. Thus, the analysis of structural properties (e.g. coordination and bond orientational order) is key to understanding disordered systems [13,17], including their electronic [18,19], elastic [20] and thermodynamics properties (e.g. phase change transitions) [21,22].

Experimentally, X-ray (e-beam and neutron) diffraction [23] and EXAFS (extended X-ray absorption fine structure) spectroscopy [24] are the most common investigation approaches for the analysis of disordered systems. In addition to these direct structural experiments, other indirect ones, such as vibrational spectroscopy (e.g. infrared and

* Corresponding author.

E-mail address: arrigo.calzolari@nano.cnr.it (A. Calzolari).

Raman scattering, inelastic neutron scattering) [25] and spin-related methods (e.g. NMR) [26] are typically used. While these methods provide general information on short range order, by measuring for example the radial distribution function or the first sharp diffraction peak (FSDP), they do not give sufficient in-depth quantitative information about local orders, such as bond polarity, folded structures, angular distortions, ring statistics and networks connectivity.

Since the non-crystalline structure cannot be determined explicitly from experiments, atomistic computer simulations, such as classical or *ab initio* molecular dynamics (MD), became of paramount relevance to overcome this drawback. Within these approaches, the amorphous models result from the use of melt-and-quench techniques, in which a sample is melt at a temperature higher than the melting temperature, and then quenched (typically to room temperature) fast enough to avoid crystallization. The mean structural properties rely on the time average properties extracted from simulated trajectories. This implies to analyze a multitude of configurations with tens to thousands of simulated atoms, an extremely time-consuming task that cannot be reliably performed manually.

In this paper, we introduce the code BELLO (Bond Element Lattice Local Order), a script-tool designed to extract and analyze local order structures in disordered materials. BELLO operates as a computationally inexpensive post-processing step that needs as input the cell dimension and the atomic positions in standard XYZ format, independently from the physical model (e.g. classical or *ab initio* MD, MonteCarlo, tight-binding) and the numerical approximations or the code used to generate the trajectories. BELLO is publicly available under the terms of the GNU General Public License, as published by the Free Software Foundation (License version 3 or any later), and it is distributed at URL website <https://github.com/behnoor-dianat/BELLO>. BELLO aims at enlarging the portfolio of the analysis tools for the study of short-range order in disordered systems [27], complementing the information, e.g., on connectivity and atomic coordination that can be derived by using other efficient codes, such as R.I.N.G.S code [28], pymatgen [29] and ChemEnv [30].

In the following we present the main technical characteristics of the code and its principal features. As prototypical application case, we present the structural analysis of GeSe and GeTe₄ amorphous chalcogenides, as resulting from Car-Parrinello molecular dynamics simulations.

2. Test cases

In order to describe the capabilities of the code, we show all along the paper the results we obtained by applying BELLO to two realistic research systems about amorphous chalcogenides, namely Ge_{0.5}Se_{0.5}, and GeTe₄. In both cases, the atomic model has been obtained from first principles molecular dynamics simulations. Time evolution is simulated using *ab initio* Car-Parrinello (CP) molecular dynamics [31], as implemented in the Quantum Espresso package [32]. The electronic structure is described within the Density functional theory (DFT) approach. The exchange-correlation functional is described by using the vdW-DF2-B86R16 formulation of generalized gradient approximation [33,34], which includes vdW-DF corrections to describe non-bonding interactions. Atomic potentials are described by ultrasoft pseudopotentials of Vanderbilt type [35]. Single particle wavefunctions (charge) are expanded in plane waves up to a kinetic energy cutoff of 30 Ry (300 Ry). The fictitious mass associated with the electronic orbital degrees of freedom is set to 600 au. The time step for molecular dynamics evolution is dt=0.17 fs. The ionic temperature is controlled by a chain of two Nosé-Hoover thermostats [36,37] with frequencies $\omega_1 = 50$ THz and $\omega_2 = 25$ THz, respectively. To fix the undesired heat transfer from the ionic to the fictitious-electronic degrees of freedom, we coupled a further Nosé-Hoover thermostat ($\omega_{el} = 100$ THz) to the electronic orbital degrees of freedom in the Car-Parrinello Lagrangian [38].

Table 1
Python libraries used in BELLO and their versions.

python libs	version
PySimpleGUI	4.56.0
Numpy	1.18.5
Pandas	1.3.5
matplotlib	3.5.1
scipy	1.7.2
Seaborn	0.11.2

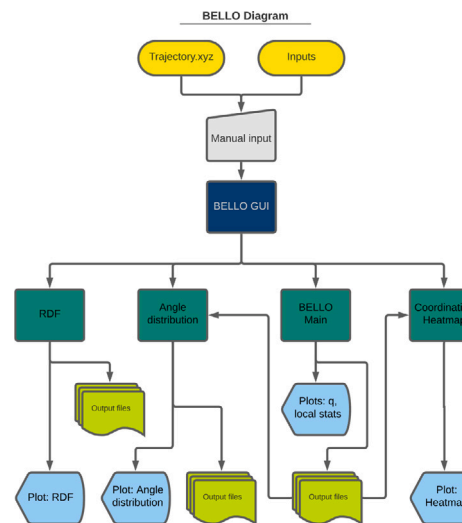


Fig. 1. Graphic illustration of BELLO structure and module dependencies.

Initial configuration of Ge_{0.5}Se_{0.5} is obtained from an amorphous model already published in the literature [27], which includes 336 atoms (168 Ge and 168 Se) per unit cell of dimension (21.30 × 21.63 × 21.11) Å³. We performed a melting-and-quenching amorphization cycle, by heating the system to 1500 K for 15 ps, followed by a cell optimization (Parrinello-Rahman) at 1200 K for 10 ps and by a cooling step to 300 K, with a rate of 100 K/ps. After quenching, a production run has been conducted at 300 K for 15ps. The model used to simulate the GeTe₄ system is composed of 270 atoms (54 Ge and 216 Te) within a cubic unit cell of dimension 20.0 Å³. The initial structure was melted by increasing the temperature up to 1200 K; the system was then quenched down to 300 K.

Notably, these examples are intended to show the properties of the BELLO code, while the physical interpretation of the two amorphous systems goes beyond the aim of this paper and will be reported elsewhere.

3. Software design

BELLO is written in python 3.7 and uses NumPy and Pandas standard libraries [39–44]. A summary of the utilized python packages and their corresponding version is reported in Table 1. BELLO is compatible with standard trajectory outputs from most of the atomistic simulation engines: it operates as post-processing tool of first-principles electronic-structure codes (e.g. QuantumEspresso, VASP, SIESTA) as well as of classical Molecular Dynamics packages (Gromacs, Lammps, DL_POLY, etc.). The only required input are the unit cell and the atomic structure trajectories in the standard XYZ format. By analyzing these trajectories in 3D real-space, BELLO systematically extracts statistical data, such as the *q*-order parameter, the extensive coordination number, the radial and angle distribution functions, the local population statistics and local order coordinates in PDB and XYZ formats, as detailed in the following.

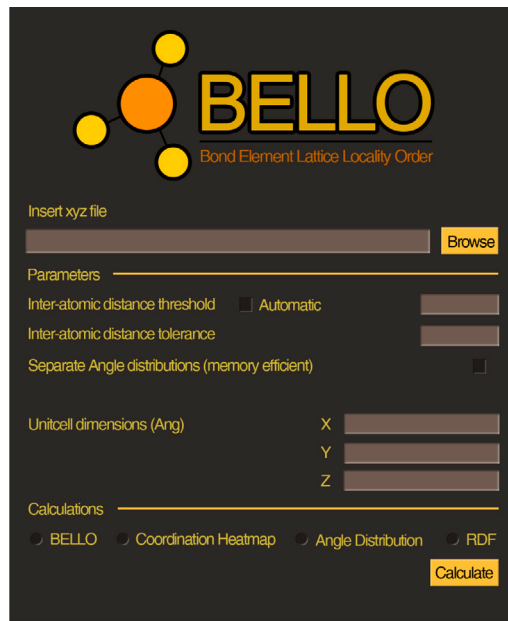


Fig. 2. Snapshot of the BELLO GUI..

4. Description of the code

BELLO is composed of five modules: four operating units and one Graphical interface, which handles input/output and code executions. Operating modules can be alternatively launched without the GUI, through simple shell command lines. The main structure of the code with the working workflow and module dependencies is shown in Fig. 1. The properties and implementation of each module is described in the following Sections.

4.1. Module: *BELLO_GUI.py*

BELLO_GUI provides a user friendly interface within python environment to interact with BELLO back-end. The GUI is implemented within the Python Integrated Development and Learning Environment (IDLE). Through the GUI (Fig. 2), users can load the computed trajectory file from the local disk, set inter-atomic distances and cell dimensions (float variables). An additional option for the segregation of angle distributions is available and useful for reduce the memory occupation of large files. Finally, by selecting options in the pop-up windows, users can run the desired modules. A progress bar with remaining/spent time is displayed while the code is being executed.

4.2. Module: *BELLO_main.py*

BELLO_main is the core engine of the code. This module automatically characterizes and extracts from the input trajectories the structural values that are used to compute the statistical parameters also by the other modules. Initially, the input file is read as a standard atomic trajectory, i.e. as a sequence of structure frames. Input pull and output push are managed by Pandas and Numpy libraries, which ensure a structured and fast data handlings. User inputs include unit cell dimensions in Å (axis are perpendicular each other by default), interatomic distances threshold (named *distance*) and interatomic distance tolerance δd , which can either be introduced manually or automatically through the GUI. In the latter case, *distance* and δd are retrieved from the analysis of radial distribution function calculations (see below). In particular, after fitting the first maximum peak with a Gaussian

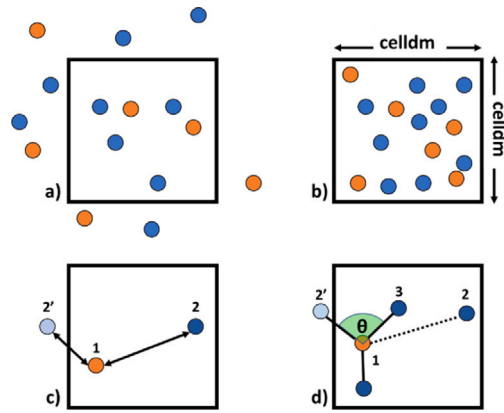


Fig. 3. Schematic representation of the applied periodic boundary conditions with atoms outside of unit cell (a) moved inside (b) the unit cell; (c) atomic distances calculated between the central atom (2) and the ligand (2'); (d) angle calculation between ligands.

function, the *distance* is chosen as the x axis position of the peak, while the tolerance is set to its width. Depending on the system, these values must be carefully chosen to account for the first neighbor shells, thus, making this step critical.

Prior to any calculation, initial periodic boundary conditions are applied on the whole system, re-allocating all the atoms inside the unit cell (Fig. 3a,b). After the reading of the input trajectory, for each frame the code generates a map of atom neighbors. This is done by a recursive loop over all atoms that, selecting one atom as the center of local order, calculates the distances to all other atoms, including periodic replica (Fig. 3c). Atom pairs that satisfy the distance criteria [45,46] are kept as local order bonds. The applied distance criteria are:

$$\Delta x_n = |a_n - a'_n| \quad (1)$$

$$distance = Min(\Delta x_n, |A_n - \Delta x_n|)$$

where $n = x, y, z$, A_n are unit cell dimensions, a_n and a'_n are the cartesian components of the atomic positions along x_n direction, respectively. The number of neighbors can vary between 0 (isolated atom) to 6 (octahedral geometries), higher coordinated assemblies are disregarded. Once the coordination map is obtained, all relevant information for local-order analysis including bond angles, bonding atom types and atomic coordinates are collected for calculation purposes. For example, Fig. 3d shows the process to evaluate the interatomic angles according to boundary conditions. The outcome is used to geometrically characterize the atomic structure through the evaluation of the following parameters.

q-order parameter and fold statistics. The *q* parameter quantifies the short-range structural order in disordered systems in terms of the atomic folding, having the tetrahedral and octahedral atomic arrangement as reference, which are typical of the cubic systems (e.g. Si, Ge). This parameter is largely used to analyze highly aggregated systems, such as amorphous semiconductors [27,47]. *q* is defined as [48]:

$$q = 1 - \frac{3}{8} \sum_{k>i} \left(\frac{1}{3} - \cos \theta_{ijk} \right)^2, \quad (2)$$

where θ_{ijk} is the angle formed between a central atom *j* and its neighboring atoms *i* and *k*. Following Eq. (2), $q = 1$ identifies a perfect tetrahedral 4-fold coordination, while $q = 0$ describes a perfect octahedral (6-fold) structure. Additional defective octahedral geometries are represented by values in the range of (-3,1). Fig. 4 shows the most relevant atomic folds and the corresponding *q* values.

The *q* parameters are calculated for each trajectory step, and further averaged over each frame and stored alongside the contributing individual values. The code collectively reports the total *q* parameters in one output file (.txt format), as well as separate files for each geometry

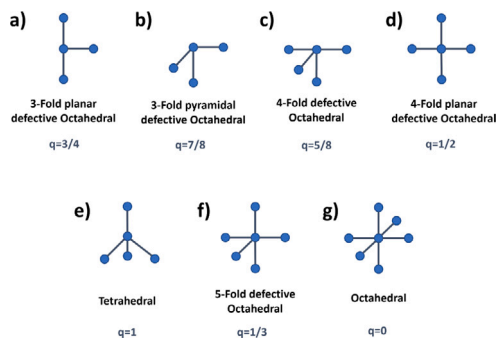


Fig. 4. Ideal form of local order geometries 3-Folds (a, b), 4-Folds (c, d), Tetrahedral (e), 5-Fold (f) and Octahedral (g), along with the corresponding q values.

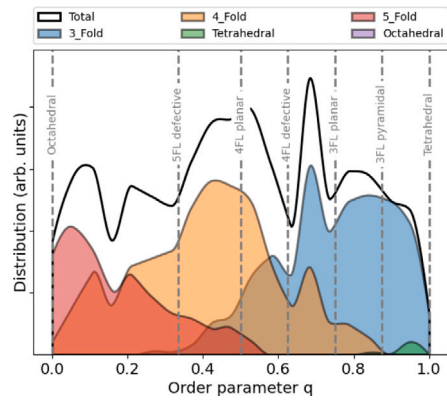


Fig. 5. q -order parameters as plotted by BELLO from $\text{Ge}_{0.5}\text{Se}_{0.5}$ trajectory. The vertical lines indicate ideal local order values, as reported in Fig. 4.

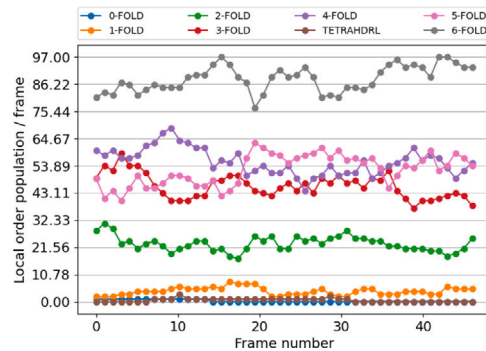


Fig. 6. Local order population statistics corresponding to the trajectory frames from molecular dynamics simulation of GeTe_4 . The plot is a standard output of BELLO_main module.

contribution (e.g. 2-fold, 3-fold, 4-fold, etc.) to the total q value. Fig. 5 shows the fold distribution resulting from the BELLO_main execution for the $\text{Ge}_{0.5}\text{Se}_{0.5}$ testbed.

BELLO collects local-order population (e.g. n -fold local structures) throughout the trajectory. This allows one to monitor the time evolution of the short-range order and the transitions to higher/lower folds during the MD simulations. The statistical data are grouped by fold-type and exported as a text output (output-local-statistics.txt). BELLO_main automatically generates a data plot at the end of the calculation, as shown in Fig. 6 in the case of GeTe_4 at room temperature.

4.2.1. PDB and XYZ output formats

The PDB (protein data bank) format is a widely used database for the three-dimensional structural data. It contains the unit cell

data as well as aggregated information about different configurations; moreover it can be read by most free visualization softwares, such as VMD [49], Avogadro [50], and Mercury [51]. BELLO adopted this format to store structure information that can be easily marked by single or group of atoms. The atom types, the XYZ coordinates, the local order type, coordination number, and the atom list numbers are saved in the PDB output file. Geometrical information and values for every extracted fold are written within the PDB columns and can be visualized by a graphics software. Fig. 7 illustrates a 3D example of polyhedral folds from the PDB output in the case of $\text{Ge}_{0.5}\text{Se}_{0.5}$ chalcogenide. Ge and Se atoms are represented by purple and yellow colors, respectively. The output file (Fig. 7, right panel) has the following format for each trajectory step: the first row refers to the central atom with number X, where the alphanumeric label (e.g. “3FL”) describes the atom folding and the number of bound atoms, reported in the following rows. In this example, the Ge-atom with number 1 is a 3-Fold atom connected to atoms number 55, 71 and 152. Fold-type and the coordinates of the other atoms follow in the list. This allows for a ready visualization of selected fold structures, whose data can be extracted by querying the corresponding label tags in the pdb file.

The atomic coordinates of selected fold geometries are also saved as output file in the standard XYZ format. Duplicate atoms emerging from bond sharing between local orders are removed in the output file.

4.3. Module: Coordination_Heatmap.py

The coordination number is defined as the number of bonded atoms to a certain atom. It is usually given as an average number for the entire system. However, for complex systems with several chemical element or with off-stoichiometry ratios, it is useful to disentangle the contributions of the single elements to the local order bonds. This makes quickly diverge the number of entries, making the results difficult to analyze. Hence, the need for manageable coordination results led us to arrange these data in the form of coordination *heat maps*, which are easily accessible through a visual analysis tool. The module distinguishes central atom and the ligand types and their population frequency by reading Output-human-readable.txt from the BELLO_main. A list of two-six predefined chemical species has to be provided as user input to distinguish and extract the selected atom types. The module computes the combination-with-repetitions $C_{(n+r-1,r)}$ of defined elements for each local order, following the expression [52]:

$$C_{(n+r-1,r)} = \frac{(n+r-1)!}{r!(n-1)!} \quad (3)$$

The distribution of these combinations are then automatically visualized via multiple coordination heat maps. Fig. 8 displays a 2-element sample output of the amorphous GeTe_4 structure.

4.4. Module: Angle_Distribution_Function.py

Complementary to the coordination heat map, the angle distribution function significantly contributes to short-range order characterization. After a successful execution of BELLO_main, all bond angles between every two ligands and a central atom are stored in the output file output-angle-distribution.txt. The Angle_Distribution_Function module calculates and plots the distribution histogram of these angles, making a more tailored representation of short-range order characteristics. A sample output for the case of GeTe_4 is presented in Fig. 9. This example corresponds to the distribution of the Ge–Te–Te angle, where the middle-Te being the central atom and the others two are the ligands. The module plots all combinations of defined species accounting for repetitions. Moreover, the graphical interface strongly reduces the redundancy of the output and the rehash of data, giving a fast and intuitive way to discern the most important bond angle contributions.

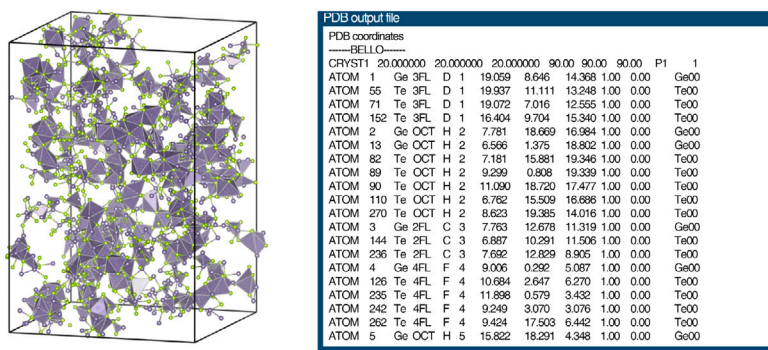


Fig. 7. Left panel) 3D visualization of octahedral folds (purple polyhedrons), tagged from the PDB output for chalcogenide $\text{Ge}_{0.5}\text{Se}_{0.5}$. Right panel) PDB output file format sample resulting from BELLO_main module for GeTe_4 . The fifth column reports the annotated local order (e.g. C 3: third extracted local order that is 2-Fold).

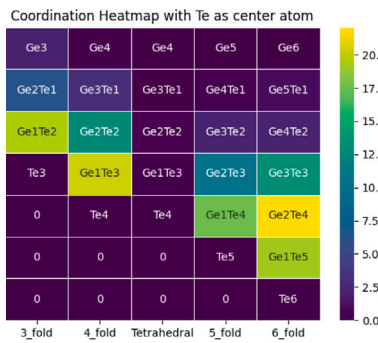


Fig. 8. Coordination heat map of GeTe_4 at 300 K, where Te is chosen as central atom. The color map refers to populations averaged over all frames.

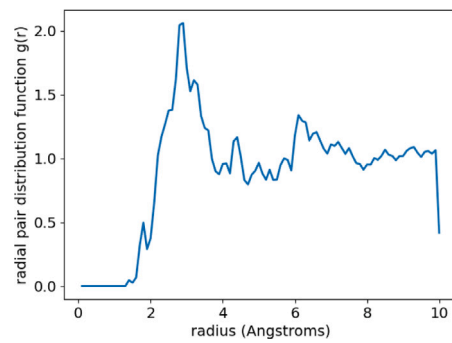


Fig. 10. Total Radial distribution function of GeTe_4 .

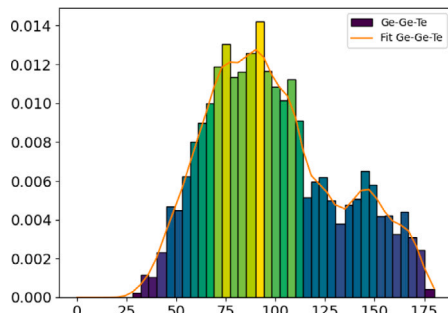


Fig. 9. Bond angle distribution function of Ge-Te-Te, from the extracted local orders of the amorphous GeTe_4 .

4.5. Module: Radial-Distribution-function.py

A simple but quantitative description of internal structure of disordered materials can be achieved via Radial Distribution Function $g(r)$ (RDF). Considering a given atom, the RDF describes the probability of finding another atom at a given distance from the central one, thus, quantifying how an atom of interest is surrounded by other atoms [53]:

$$g(r) = \frac{V}{4\pi r^2 N^2} \sum_i \sum_{j \neq i} \delta(r - r_{ij}), \quad (4)$$

where V is unit cell volume, N is the total number of atoms inside unit cell, i and j represent atoms A and B respectively, and r_{ij} is the interatomic distance. The radial distribution function is calculated for each trajectory step and eventually averaged over all frames. In an ideal gas which has no internal structure, RDF yields a constant number [$g(r) = 1$], while a crystalline solid with periodically located atoms, results in a sharply picked RDF at the position of atoms and is

Table 2

Prerequisites of BELLO modules for calculation, angle distribution function and coordination heatmap use output files generated by BELLO_main.

Module	XYZ file	Interatomic dist.	Cell dim.	Species
BELLO_main	✓	✓	✓	
Angle Distribution				✓
Radial Distribution	✓		✓	
Coordination Heatmap				✓

zero in between. Starting with the standard atomic structure trajectory and after the application of the periodic boundary condition (main module), the RDF module calculates the interatomic distances between the selected chemical elements. Then, conditional probability density of finding an atom B from a fixed atom A is at the coordinate origin is computed by $g(r)$. RDF is calculated for each frame and averaged over the trajectory steps. Fig. 10 presents $g(r)$ output for Ge and Te atoms in case GeTe_4 .

5. Installation, input and output structure

BELLO does not require any installation or specific setup, provided that Python 3.7 as well as specified libraries in Table 1 are installed on the system. A brief README file with installation and running commands is available online in the github repository of the code. BELLO_GUI handles user inputs for different modules. A list of user inputs and required data are summarized in Table 2. The input file must be in the same directory of the modules. Output files are stored in the same directory with the text file extension(.txt). The files are fully structured and easy to read. Generated graphics can be exported in the several formats (e.g. jpeg, png, pdf). Colors choice, labels and graphical definitions can be set by the user to best match the quality standards required by publication journals.

6. Conclusion

By introducing BELLO, we provided a powerful user-friendly post-processing script-tool, created for systematic analysis and extraction of structural characteristics of disordered and amorphous systems. The code was developed with a focus on short-range order characterization and requires minimal input setup and computational resources. The graphical interface of BELLO takes advantage of the modular nature and the flexibility of the code to provide users with tailored results and plots, thus, accelerating the post-processing analysis of complex materials.

CRediT authorship contribution statement

Behnoor Dianat: Implemented the code, Contributed in writing the manuscript. **Francesco Tavanti:** Did the analysis, Contributed in writing the manuscript. **Andrea Padovani:** Did the analysis, Contributed in writing the manuscript. **Luca Larcher:** Coordinated the project, Contributed in writing the manuscript. **Arrigo Calzolari:** Coordinated the project, Contributed in writing the manuscript.

Declaration of competing interest

The authors declare that they have no known competing financial interests or personal relationships that could have appeared to influence the work reported in this paper.

Data availability

All the *ab initio* data are freely available to the public as part of the <https://materialscloud.org> online repository.

Acknowledgment

This work was supported in part by European Commission through H2020-NMBP-TO-IND project GA n. 814487 (INTERSECT).

References

- [1] J. Zhu, Z. Yu, G.F. Burkhard, C.-M. Hsu, S.T. Connor, Y. Xu, Q. Wang, M. McGhee, S. Fan, Y. Cui, Optical absorption enhancement in Amorphous silicon nanowire and nanocone arrays, *Nano Lett.* 9 (1) (2009) 279–282.
- [2] C.-M.H.Z.Y.S.F. Jia Zhu, Y. Cui, Nanodome solar cells with efficient light management and self-cleaning, *Nano Lett.* 10 (2010) 1–6.
- [3] X. Gai, D.-Y. Choi, B. Luther-Davies, Negligible nonlinear absorption in hydrogenated amorphous silicon at 155 μm for ultra-fast nonlinear signal processing, *Opt. Exp.* 22 (8) (2014) 9911–9948.
- [4] K. Nomura, H. Ohta, A. Takagi, T. Kamiya, M. Hirano, H. Hosono, Room-temperature fabrication of transparent flexible thin-film transistors using amorphous oxide semiconductors, *Nature* 432 (2004) 488–492.
- [5] T. Kamiya, K. Nomura, H. Hosono, Present status of amorphous in-Ga-Zn-O thin-film transistors, *Sci. Tech. Adv. Mater.* 11 (4) (2010) 044305.
- [6] M.G. Kuzyk, *Polymer Fiber Optics*, CRC Press Taylor & Francis Group, Boca Raton FL, USA, 2007.
- [7] K. Peters, Polymer optical fiber sensors—a review, *Smart Mater. Struct.* 20 (2010) 013002.
- [8] T. Ohta, Phase-change optical memory promotes the DVD optical disk, *J. Opt. Adv. Mater.* 3 (3) (2001) 609–626.
- [9] M. Wuttig, N. Yamada, Phase-change materials for rewriteable data storage, *Nature Mater.* 6 (11) (2009) 824–832.
- [10] G.W. Burr, M.J. Breitwisch, M. Franceschini, D. Garetto, K. Gopalakrishnan, B. Jackson, B. Kurdi, C. Lam, L.A. Lastras, A. Padilla, B. Rajendran, S. Raoux, R.S. Shenoy, Phase change memory technology, *J. Vac. Sci. Technol. B* 28 (2) (2010) 223–262.
- [11] P.A. Lee, T.V. Ramakrishnan, Disordered electronic systems, *Rev. Modern Phys.* 57 (2) (1985) 287–337, Sistemi metallici, Anderson localization, definizione mobility Gap.
- [12] D.J. Thouless, Electrons in disordered systems and the theory of localization, *Phys. Rep.* 13 (3) (1974) 93–142.
- [13] P. Häussler, Interrelations between atomic and electronic structures—liquid and amorphous metals as model systems, *Phys. Rep.* 222 (2) (1992) 65–143.
- [14] S.R. Ovshinsky, D. Adler, Local structure, bonding, and electric properties of covalent amorphous semiconductors, *Contemp. Phys.* 19 (1978) 109–126.
- [15] M. Popescu, *Structure, Defects and Electronic Properties of Amorphous Semiconductors*, John Wiley & Sons, Ltd, Weinheim, Germany, 2003.
- [16] P.J. Steinhardt, D.R. Nelson, M. Ronchetti, Bond-orientational order in liquids and glasses, *Phys. Rev. B* 28 (2) (1983) 784–805.
- [17] Z.H. Stachurski, On structure and properties of amorphous materials, *Materials* 4 (9) (2011) 1564–1598.
- [18] K. Moorjani, C. Feldman, Electrical properties of amorphous semiconductors, *Rev. Modern Phys.* 36 (4) (1964) 1042–1049.
- [19] D. Adler, H.K. Henisch, S.N. Mott, The mechanism of threshold switching in amorphous alloys, *Rev. Modern Phys.* 50 (2) (1978) 209–220.
- [20] S. Alexander, Amorphous solids: their structure, lattice dynamics and elasticity, *Phys. Rep.* 296 (2–4) (1998) 65–236.
- [21] F.H. Stillinger, Supercooled liquids, glass transitions, and the Kauzmann paradox, *J. Chem. Phys.* 88 (1) (1988) 7818–7825.
- [22] L. Berthier, G. Biroli, Theoretical perspective on the glass transition and amorphous materials, *Rev. Modern Phys.* 83 (2) (2011) 587–645.
- [23] G.N. Greaves, S. Sen, Inorganic glasses, glass-forming liquids and amorphizing solids, *Adv. Phys.* 56 (2007) 1–166.
- [24] M. Vaccari, G. Garbarino, S.N. Yannopoulos, K.S. Andrikopoulos, S. Pasquarelli, High pressure transition in amorphous As₂S₃ studied by EXAFS, *J. Chem. Phys.* 131 (2009) 224502.
- [25] S.N. Yannopoulos, K.S. Andrikopoulos, Raman scattering study on structural and dynamical features of noncrystalline selenium, *J. Chem. Phys.* 121 (2004) 4747–4758.
- [26] R. Böhmer, G. Diezemann, G. Hinze, E. Rössler, Dynamics of supercooled liquids and glassy solids, *Progr. Nucl. Magn. Res. Spec.* 39 (2001) 191–267.
- [27] F. Tavanti, B. Dianat, A. Catellani, A. Calzolari, Hierarchical short-and medium-range order structures in amorphous Ge x Se1-x for selectors applications, *ACS Appl. Electr. Mater.* 2 (9) (2020) 2961–2969.
- [28] S. Le Roux, P. Jund, Ring statistics analysis of topological networks: New approach and application to amorphous GeS₂ and SiO₂ systems, *Comput. Mater. Sci.* 49 (1) (2010) 70–83.
- [29] S.P. Ong, W.D. Richards, A. Jain, G. Hautier, M. Kocher, S. Cholia, D. Gunter, V.L. Chevrier, K.A. Persson, G. Ceder, Python materials Genomics (pymatgen): A robust, open-source python library for materials analysis, *Comput. Mater. Sci.* 68 (2013) 314–319, <http://dx.doi.org/10.1016/j.commatsci.2012.10.028>, URL <https://www.sciencedirect.com/science/article/pii/S0927025612006295>.
- [30] Z. Rong, D. Kitchev, P. Canepa, W. Huang, G. Ceder, An efficient algorithm for finding the minimum energy path for cation migration in ionic materials, *J. Chem. Phys.* 145 (7) (2016) 074112.
- [31] R. Car, M. Parrinello, Unified approach for molecular dynamics and density-functional theory, *Phys. Rev. Lett.* 55 (1985) 2471–2474, <http://dx.doi.org/10.1103/PhysRevLett.55.2471>, URL <https://link.aps.org/doi/10.1103/PhysRevLett.55.2471>.
- [32] P. Giannozzi, S. Baroni, N. Bonini, M. Calandra, R. Car, C. Cavazzoni, D. Ceresoli, G.L. Chiarotti, M. Cococcioni, I. Dabo, A.D. Corso, S. de Gironcoli, S. Fabris, G. Fratesi, R. Gebauer, U. Gerstmann, C. Gougoussis, A. Kokalj, M. Lazzeri, L. Martin-Samos, N. Marzari, F. Mauri, R. Mazzarello, S. Paolini, A. Pasquarello, L. Paulatto, C. Sbraccia, S. Scandolo, G. Sclauzero, A.P. Seitsonen, A. Smogunov, P. Umari, R.M. Wentzcovitch, QUANTUM ESPRESSO: a modular and open-source software project for quantum simulations of materials, *J. Phys.: Condens. Matter* 21 (39) (2009) 395502, <http://dx.doi.org/10.1088/0953-8984/21/39/395502>.
- [33] T. Thonhauser, S. Zuluaga, C.A. Arter, K. Berland, E. Schröder, P. Hyldgaard, Spin signature of nonlocal correlation binding in metal-organic frameworks, *Phys. Rev. Lett.* 115 (2015) 136402, <http://dx.doi.org/10.1103/PhysRevLett.115.136402>, URL <https://link.aps.org/doi/10.1103/PhysRevLett.115.136402>.
- [34] D.C. Langreth, B.I. Lundqvist, S.D. Chakarova-Kack, V.R. Cooper, M. Dion, P. Hyldgaard, A. Kelkkanen, J. Kleis, L. Kong, S. Li, P.G. Moses, E. Murray, A. Puzder, H. Rydberg, E. Schroeder, T. Thonhauser, A density functional for sparse matter, *J. Phys. 21* (8) (2009) 084203, <http://dx.doi.org/10.1088/0953-8984/21/8/084203>.
- [35] D. Vanderbilt, Soft self-consistent pseudopotentials in a generalized eigenvalue formalism, *Phys. Rev. B* 41 (11) (1990) R7892–R7895.
- [36] S.A. Nosé, Unified formulation of the constant temperature molecular dynamics methods, *Phys. Rev. Lett.* 81 (1) (1984) 511–519.
- [37] W. Hoover, Canonical dynamics: Equilibrium phase-space distributions, *Phys. Rev. A* 31 (3) (1985) 1695–1697.
- [38] G. Pastore, E. Smargiassi, F. Buda, Theory of ab initio molecular-dynamics calculations, *Phys. Rev. A* 44 (1991) 6334–6347, <http://dx.doi.org/10.1103/PhysRevA.44.6334>, URL <https://link.aps.org/doi/10.1103/PhysRevA.44.6334>.
- [39] C.R. Harris, K.J. Millman, S.J. van der Walt, R. Gommers, P. Virtanen, D. Cournapeau, E. Wieser, J. Taylor, S. Berg, N.J. Smith, R. Kern, M. Picus, S. Hoyer, M.H. van Kerwijk, M. Brett, A. Haldane, J.F. del Río, M. Wiebe, P. Peterson, P. Gérard-Marchant, K. Sheppard, T. Reddy, W. Weckesser, H. Abbasi, C. Gohlke, T.E. Oliphant, Array programming with NumPy, *Nature* 585 (7825) (2020) 357–362, <http://dx.doi.org/10.1038/s41586-020-2649-2>.
- [40] W. McKinney, Data structures for statistical computing in python, in: S. van der Walt, J. Millman (Eds.), *Proceedings of the 9th Python in Science Conference*, 2010, pp. 56–61, <http://dx.doi.org/10.25080/Majora-92bf1922-00a>.

- [41] T. pandas development team, pandas-dev/pandas: Pandas, Zenodo, 2020, <http://dx.doi.org/10.5281/zenodo.3509134>.
- [42] J.D. Hunter, Matplotlib: A 2D graphics environment, *Comput. Sci. Eng.* 9 (3) (2007) 90–95, <http://dx.doi.org/10.1109/MCSE.2007.55>.
- [43] P. Virtanen, R. Gommers, T.E. Oliphant, M. Haberland, T. Reddy, D. Cournapeau, E. Burovski, P. Peterson, W. Weckesser, J. Bright, S.J. van der Walt, M. Brett, J. Wilson, K.J. Millman, N. Mayorov, A.R.J. Nelson, E. Jones, R. Kern, E. Larson, C.J. Carey, I. Polat, Y. Feng, E.W. Moore, J. VanderPlas, D. Laxalde, J. Perktold, R. Cimrman, I. Henriksen, E.A. Quintero, C.R. Harris, A.M. Archibald, A.H. Ribeiro, F. Pedregosa, P. van Mulbregt, SciPy 1.0 Contributors, SciPy 1.0: Fundamental algorithms for scientific computing in python, *Nature Methods* 17 (2020) 261–272, <http://dx.doi.org/10.1038/s41592-019-0686-2>.
- [44] M.L. Waskom, Seaborn: statistical data visualization, *J. Open Source Softw.* 6 (60) (2021) 3021, <http://dx.doi.org/10.21105/joss.03021>.
- [45] D. Frenkel, B. Smit, *Understanding Molecular Simulation: From Algorithms to Applications*, vol. 1, Elsevier, 2001.
- [46] F.J. Vesely, *Computational Physics*, Springer, 1994.
- [47] G.C. Sosso, G. Miceli, S. Caravati, J. Behler, M. Bernasconi, Neural network interatomic potential for the phase change material GeTe, *Phys. Rev. B* 85 (17) (2012) 174103.
- [48] J.R. Errington, P.G. Debenedetti, Relationship between structural order and the anomalies of liquid water, *Nature* 409 (6818) (2001) 318–321.
- [49] W. Humphrey, A. Dalke, K. Schulten, VMD: visual molecular dynamics, *J. Mol. Graph.* 14 (1) (1996) 33–38.
- [50] M.D. Hanwell, D.E. Curtis, D.C. Lonie, T. Vandermeersch, E. Zurek, G.R. Hutchison, Avogadro: An advanced semantic chemical editor, visualization, and analysis platform, *J. Cheminformatics* 4 (2012) 17.
- [51] C.F. Macrae, I. Sovago, S.J. Cottrell, P.T.A. Galek, P. McCabe, E. Pidcock, M. Platings, G.P. Shields, J.S. Stevens, M. Towler, P.A. Wood, Mercury 4.0: from visualization to analysis, design and prediction, *J. Appl. Cryst.* 53 (2020) 226–235.
- [52] E. Gossett, *Discrete Mathematics with Proof*, Wiley, 2009, URL <https://books.google.it/books?id=NuFeW8N2hlkC>.
- [53] F. Kohler, *The Liquid State*, Verlag Chemie GmbH, Weinheim/Bergstr, 1972.